Soft Matter

Viscoelasticity in associating oligomers and polymers: experimental test of the bond lifetime renormalization model

Journal:	*Soft Matter*
Manuscript ID	SM-ART-09-2019-001930.R1
Article Type:	Paper
Date Submitted by the Author:	27-Nov-2019
Complete List of Authors:	Ge, Sirui; University of Tennessee, Materials Science and Engineering Tress, Martin; Max-Planck-Institut fur Polymerforschung, ; University of Tennessee Knoxville College of Arts and Sciences, Department of Chemistry Xing, Kunyue; University of Tennessee, Chemistry Cao, Pengfei; Oak Ridge National Laboratory, chemical science division Saito, Tomonori; Oak Ridge National Laboratory, Chemical Sciences Division Sokolov, Alexei; University of Tennessee, Department of Chemistry and Physics & Astronomy

Viscoelasticity in associating oligomers and polymers: experimental test of the bond lifetime renormalization model

Sirui Ge[1]†, Martin Tress[2]†, Kunyue Xing[2], Peng-Fei Cao[3], Tomonori Saito[3], and Alexei P. Sokolov[2, 3]*
[†] The two authors contributed equally to this work.
[*] Corresponding author: Alexei P. Sokolov (sokolov@utk.edu)

[1] *University of Tennessee, Knoxville, Department of Materials Science, Knoxville, Tennessee 37996, United States*
[2] *University of Tennessee, Knoxville, Department of Chemistry, Knoxville, Tennessee 37996, United States*
[3] *Oak Ridge National Laboratory, Chemical Sciences Division, Oak Ridge, Tennessee 37831, United States*

Abstract
Recent findings that the association bond lifetimes τ_{α^*} in associating polymers diverge from their supramolecular network relaxation times τ_c challenge past theories. The bond lifetime renormalization proposed by Rubinstein and coworkers [Stukalin et al. *Macromolecules* 46 (2013) 7525] provides a promising explanation. To examine systematically its applicability, we employ shear rheology and dielectric spectroscopy to study telechelic associating polymers with different main chain (polypropylene glycol and polydimethylsiloxane), molecular weight (below entanglement molecular weight) and end groups (amide, and carboxylic acid) which form dimeric associations by hydrogen bonding. The separation between τ_c (probed by rheology) and τ_{α^*} (probed by dielectric spectroscopy) strongly increases with chain length as qualitatively predicted by the model. However, to describe the increase quantitatively, a transition from Rouse to reptation dynamics must be assumed. This suggests that dynamics of super-chains must be considered to properly describe the transient network.

Introduction
Supramolecular polymers employ functional groups which act as stickers to form non-covalent bonds and generate a transient network structure[1, 2]. Different types of interactions may be used, e.g. hydrogen (H-) bonding[3, 4], ionic bonding[5, 6], metal-ligand bonding[7], π-π interaction and host-guest interaction[8]. Compared to conventional polymers, these materials exhibit unusual and remarkable properties ranging from increasing glass transition temperatures with decreasing molecular weight[9], to super-stretchability[10], self-healing abilities[11-14] and shape memory mechanisms[15, 16]. In order to benefit from these extraordinary functionalities and incorporate them into applied science, it is of paramount importance to understand how the association impacts macroscopic properties.

Since several decades associating polymers with multiple stickers randomly distributed along the polymer chains have been studied in both melt[17, 18] and solution[19-21]. Recently, also much better

defined systems like telechelic polymers are in focus[22-25] [26, 27]. Due to the mechanical robustness established by the supramolecular network, many studies employ rheological measurements. Several models were proposed to explain the experimental results on a molecular level, such as the Sticky Rouse model[28] and the Reversible Gelation model[29]. A central parameter in these descriptions is the activation energy E_a required to dissociate the bond between stickers[30]. E.g. Tanaka and Edwards[31, 32] and Indei[33, 34] proposed models to calculate this energy for cluster associations and pairwise associations, respectively, from the characteristic relaxation times revealed in rheology. It is basically agreed that the structural relaxation time τ_S (segmental relaxation time in polymers) is the pre-factor in an Arrhenius type equation[28, 30] describing the temperature dependence of the characteristic dissociation time τ_b of the supramolecular network

$$\tau_b(T) = \tau_S(T)\exp\left(\frac{E_a}{RT}\right) \quad (1)$$

where R is the gas constant. The earlier rheological studies considered that the terminal relaxation time τ_c in shear modulus spectra reflects the characteristic time of the sticker dissociation τ_b. However, the recent investigations combining rheology and dielectric spectroscopy challenged this interpretation[35, 36].

Dielectric spectroscopy[37] can provide insight not only into the orientational dynamics but also into association behavior of such polymers, because the dissociation of stickers is accompanied by a change in the dipole moment (since the stickers are often polar groups). This means that the dissociation can be observed in dielectric spectra and is commonly referred to as α*-relaxation[38] with the characteristic relaxation time $\tau_{\alpha*}$. Additionally, dielectric spectroscopy is also a common method to probe the segmental relaxation of polymers[37]. Hence, similarly to rheology, also dielectric spectroscopy can be used to trace the relevant processes in associating polymers[39]. In recent studies of entangled polyisoprene randomly functionalized with urazole groups, it has been found that the rheological terminal relaxation time τ_c is several orders slower than the sticker dissociation time probed by dielectric spectroscopy $\tau_{\alpha*}$[35, 36]. The authors explained this observation with the concept of lifetime renormalization proposed by Stukalin et al.[40].
This model differentiates between the actual lifetime of a bond τ_b describing the characteristic time of sticker dissociation, and the renormalized bond lifetime τ_b^{renm} which denotes the characteristic time of structural reorganization of the network, i.e. the event when a sticker changes its bond partner. The former produces a change in the dipole moment because each dissociation and association event changes the dipole moment, and therefore is detected by dielectric spectroscopy. However, if the dissociated stickers re-associate back to their original partners, no stress relaxation occurs. Only the change of the partners, i.e. τ_b^{renm}, is relevant for mechanical stress relaxation[41]. The model predicts that only under certain conditions these two will be identical. The decisive parameter is the bond strength quantified by its activation energy E_a, and in the framework of the model, three regimes are discriminated: in the weak regime, $E_a < k_B T \ln N$ (N is the number of segments per telechelic chain), the association can be neglected while only in the strong regime, $E_a > 2\, k_B T \ln N$, bond dissociation and stress relaxation are approximately identical. For the intermediate regime, which is characterized by the condition

$k_B T \ln N < E_a < 2\, k_B T \ln N$, a more complex relaxation mechanism is suggested with two relevant contributions to the renormalized bond lifetime[40]: i) after dissociation the sticker starts a random walk; since the walk is compact, there is a significant chance that the sticker returns to its former partner J times and remains associated with it for τ_b each time, before (ii) the volume explored by the random walk is large enough for the sticker to encounter another free chain-end (sticker). The additional time τ_{open} denotes the time the sticker spends on the random walks until it associates with a new bond partner:

$$\tau_b^{renm} = J(\tau_{open})\tau_b + \tau_{open} \quad (2)$$

Apparently, τ_{open} as well as J depend on the concentration of (open) stickers in the system which in the case of telechelic chains can be described by the length of these chains[40]. Considering the assignments $\tau_b = \tau_{\alpha*}$ and $\tau_b^{renm} = \tau_c$, this model explains at least on a qualitative level why the terminal relaxation time from rheological measurements is often larger than the α*-relaxation time deduced from dielectric data.

Obviously, τ_{open} increases with increasing distance between stickers along the chain (i.e. chain length for telechelics). Accordingly, also J grows with τ_{open} since a longer diffusion path provides more occasions for a return to the origin. This was quantified by approximating the number of returns as the ratio of the average number of steps that an open sticker must diffuse to reach its new partner and the average number of segmental volumes that are explored during this diffusion[40]. While initially the model considered only diffusion driven by Rouse dynamics, i.e. the sticker mean-square displacement $\langle r(t)^2 \rangle \propto t^x$ with $x = 1/2$, a generalized version[35, 36] introduces an adjustable exponent x to describe the time dependence of the free chain-end $\langle r(t)^2 \rangle$. This allows to consider Rouse ($x = 1/2$) or reptation ($x = 1/4$) dynamics, and also transitional behavior (i.e. it considers the impact of entanglements on chain dynamics)

$$\langle \Delta r_{open}^2 \rangle = b^2 \left(\frac{\tau_{open}}{\tau_S} \right)^x \quad (3)$$

Here, Δr_{open} is the average distance between two open stickers in the system; it has been shown that it is a function of the activation energy of the sticker dissociation[40]. This enables to link τ_{open} to the number of segments N of the chain the sticker is attached to, and consequently to the number of returns to its initial partner J [35, 36].

$$J = \left[N \exp\left(\frac{E_a}{RT} \right) \right]^{\left(\frac{1}{3x} - \frac{1}{2} \right)} \quad (4)$$

With eq. (4) the renormalized bond lifetime can be expressed as[35, 36]

$$\tau_b^{renm}(T) = \tau_S(T) N^{\frac{1}{3x}} \exp\left(\frac{E_a}{3xRT} \right) \left[N^{-\frac{1}{2}} \exp\left(\frac{E_a}{2RT} \right) + 1 \right] \quad (5)$$

which links the segmental relaxation time, the terminal relaxation time, the activation energy of associations, the chain length, and the type of chain-end diffusion.

To provide thorough test of the lifetime renormalization model, we utilized both rheology and dielectric spectroscopy to probe the characteristic relaxation times of several telechelic polymers with different chain length (all below the entanglement molecular weight) and associating groups

that form dimeric associations via H-bonding. We find that the separation between terminal relaxation time and sticker dissociation time ranges from less than one decade to about 4 decades and depends strongly on molecular weight (MW) and activation energy of the end group dissociation. The model of lifetime renormalization as generalized by Gold et al.[35, 36] allows the determination of the diffusion exponent x as fit parameter from eq. (5), which exhibits a systematic transition from $x \sim 0.5$ (Rouse dynamics) to $x \sim 0.25$ (reptation dynamics) with increasing MW. This transition appears for chains with MW well below the entanglement M_e, which suggests the formation of super-chains with an effective MW above M_e. According to this analysis, the generalized model of lifetime renormalization seems to describe the behavior of associating telechelics quantitatively; though, a definite verification requires means to check independently the extracted values of the diffusion exponent x and the number of returns J.

Material & Methods

Telechelic polypropylene glycol (PPG) terminated with amide groups (PPG-NH_2) was received from Scientific Polymer Products, Inc. and Sigma-Aldrich, respectively. Telechelic PPG terminated with carboxylic acid groups and amino groups in the alkyl-linker (PPG-COOH) was synthesized from PPG-NH_2 as described in the previous publication[42]. Telechelic polydimethylsiloxane (PDMS) terminated with amide groups (PDMS-NH_2) was purchased from Gelest. Telechelic PDMS terminated with carboxylic acid groups and a thio-ether group in the alkyl-linker (PDMS-S-COOH) was synthesized from telechelic vinyl terminated PDMS (Gelest) and 3-Mercaptopropionic acid (used as received from Sigma Aldrich). To give one example, 3 g (0.5 mmol) of vinyl terminated PDMS with a MW of 6000 g/mol and 0.2123 g (2 mmol) 3-Mercaptopropionic acid were dissolved in 10 ml anhydrous toluene (used as received from Sigma Aldrich) and degassed by argon for half an hour. 2,2'-Azobis(2-methylpropionitrile) (AIBN) was purchase from Sigma-Aldrich and recrystallized by methanol. Then, 0.041 g (0.25 mmol) of the recrystallized AIBN were dissolved in 3 ml toluene and added to the polymer mixture. After degassing by argon for another 10 min, the mixture was heated to 65 °C and kept at this temperature overnight (Scheme 1) under a pure argon atmosphere. After evaporation of the solvents, the product was purged with hexane to remove the AIBN. Subsequently, the hexane was evaporated and a dialysis against dichloromethane (used as received from VMR Analytical) using a benzoylated dialysis membrane was performed to remove low molecular weight impurities. The quantitative modification of the end groups was verified by ^{1}H NMR for all samples (Figs. S1 & S2). For each material several MWs were obtained (Table 1). The names of the samples consist of the backbone, end group and degree of polymerization (DP) of the main chain; e.g. PPG-NH_2-6 means the PPG chain with NH_2 end groups and $DP = 6$.

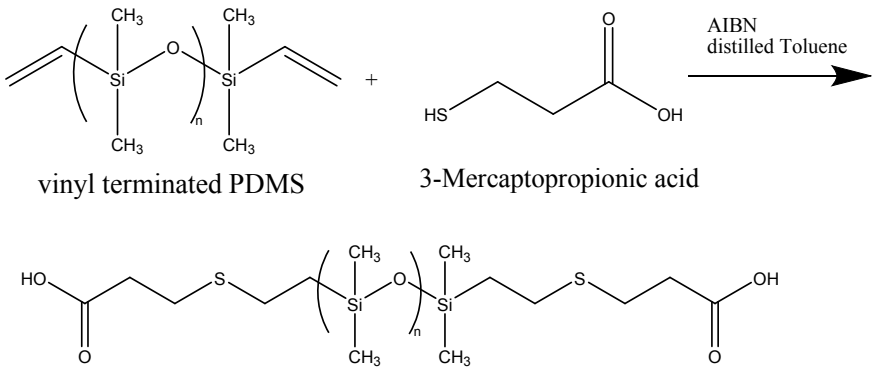

Scheme 1: Synthesis of carboxylic acid-terminated poly(dimethylsiloxane) (PDMS-S-COOH) from the vinyl terminated poly(dimethylsiloxane).

Table 1: Degree of polymerization *DP*, total number-averaged MW M_n including end-groups, as well as main chain M_n (excluding end-groups), number of Kuhn segments *N*, and glass transition temperature T_g of the studied polymers.

Polymer	***DP***	***M*n [g/mol] (total)**	***M*n [g/mol] (main chain)**	***N***	***T*g (DSC)**
PPG-NH_2-6	6	480	348	3	194
PPG-NH_2-33	33	2046	1914	17	199
PPG-NH_2-67	67	4018	3886	35	199
PPG-COOH-6	6	680	348	3	246
PPG-COOH-33	33	2246	1914	17	218
PPG-COOH-67	67	4218	3886	35	207
PDMS-NH_2-22	22	1738	1622	7	153
PDMS-NH_2-50	50	3816	3700	16	150
PDMS-NH_2-74	74	5592	5476	23	149
PDMS-S-COOH-13	13	1228	962	4	168
PDMS-S-COOH-83	83	6408	6142	26	149

Differential scanning calorimetry (DSC) was performed using a Q-1000 differential scanning calorimeter (TA Instruments). All the samples were dried in a vacuum oven for several days in order to remove remaining solvent and moisture, and subsequently sealed in hermetic aluminum pans. Scans were performed with a rate of 10 K/min, for PPG-COOH, PPG-NH_2 and PPG-OH in a temperature range from 150 K to 350 K, and for PDMS-S-COOH and PDMS-NHCO-COOH in a range from 113 K to 376 K. Before the first run, each sample was equilibrated at the highest temperature for 5 minutes. Two subsequent cooling and heating cycles were conducted to verify reproducibility and to eliminate the thermal history. The glass transition temperature (T_g) was determined from the middle point of the respective step in the heat flow.

Broadband dielectric spectroscopy (BDS) measurements were conducted with an Alpha-A impedance analyzer connected to a Quatro Cryosystem temperature controller (both from Novocontrol) in a frequency range from 10^{-2} – 10^{7} Hz. Thermalized in a dry nitrogen flow, the maximum permitted deviation in temperature was 0.2 K with an equilibration time of at least 10 minutes before recording each spectrum. Prior to the measurement, each sample was dried according to the sample protocol described for DSC measurements. All PPG samples were prepared in a parallel-plate dielectric cell made of sapphire and invar steel particularly designed for the investigation of liquids[43]. The electrodes of the cell have a diameter of 12 mm and a separation of 49 μm; the capacity of the empty cell is 20 pF. The PDMS samples were measured in a capacitor composed of two gold-plated electrodes of 20 mm diameter separated by a Teflon spacer of 34.4 μm thickness.

Small amplitude oscillatory shear (SAOS) measurements were conducted with the strain-controlled mode of an AR2000ex rheometer (TA Instruments) in the angular frequency range of 10^{2}-10^{-1} rad/s utilizing a parallel plate geometry. Plate diameters of 4 and 8 mm were employed depending on the magnitude of the shear modulus. The gap distance between the top and bottom plate was approximately 500 μm and kept constant throughout the temperature range. Prior to the measurement each sample was dried as described for the DSC measurements. A strain sweep was conducted before each spectral sweep to determine the appropriate strain keeping the SAOS in the linear regime. Before each scan, the samples were thermally equilibrated for 10 minutes, the maximum permitted temperature deviation was 0.2 K.
Zero shear viscosity measurements were performed with the same AR2000ex rheometer. For temperatures at which the viscosity was large, i.e. $\eta_0 > 10^5$ Pa s, the samples were measured with a conical plate of 25 mm diameter, a cone angle of 2°, and a truncation of 58 μm. In these cases, the low-frequency-limit of the terminal relaxation of SAOS measurements was used to estimate the viscosity according to $\eta_0 = \lim_{\omega \to 0} G''/\omega$. Lower values of $\eta_0 < 10^5$ Pa s were determined from measurements conducted with parallel plates of 8 mm diameter and a distance of ~800 μm by continuous ramp measurements with a shear rate of 10 rad/s.

Results

Differential scanning calorimetry

The T_g of the samples with *DP* of 50 or larger (i.e. MW > 3 kg/mol) for both polymers appears to be independent of the type of end-groups[39, 42]. For shorter chains, two different trends are observed (Table 1): i) functionalization with -COOH end groups strongly increases T_g as *DP* decreases for both PPG and PDMS, and in the latter chain also for -NH_2 end groups; ii) -NH_2 end groups result in an almost *DP* independent T_g in PPG. Only a slight decrease from the high-MW-value is observed for the shortest PPG-NH_2. The latter is a result of the much weaker chain end interactions which can just compensate the mobility enhancement due to the increased mobility inherent to chain ends. Furthermore, in some of the PDMS samples crystallization (~210 K) and melting peaks (~230 K) were found. However, these features are neither in the scope of this manuscript nor do they happen in the temperature range of the processes under study here; hence, they will not be discussed further.

Dielectric spectroscopy

The dielectric spectra of PDMS-S-COOH-13 exhibit two relaxations in the investigated temperature and frequency range, while those of PDMS-S-COOH-83 show three relaxations (Fig. 1). Fits of a sum of two and three Havriliak-Negami functions[44], respectively, were used to extract the characteristic mean relaxation times. In both samples, the peak occurring at the lowest temperatures and highest frequencies follows the Vogel-Fulcher-Tammann (VFT) equation[41]:

$$\tau(T) = \tau_0 \exp\left(\frac{B}{T - T_0}\right) \quad (6)$$

with the limiting relaxation time τ_0, the parameter B, and the Vogel temperature T_0. The extrapolation of the fitted curve to a relaxation time of $\tau = 100$ s coincides with the calorimetric T_g[39, 42], clearly indicating that the fastest relaxation process represents the segmental relaxation. For the short chains used here, the segmental relaxation time exhibits molecular weight dependence, which is also reflected in the change of T_g with MW (Table 1). These observations are similar to the findings of other end-functionalized PDMS (Fig. S3) and PPG samples (Fig. S4) published elsewhere[42] which also enter the following analysis.

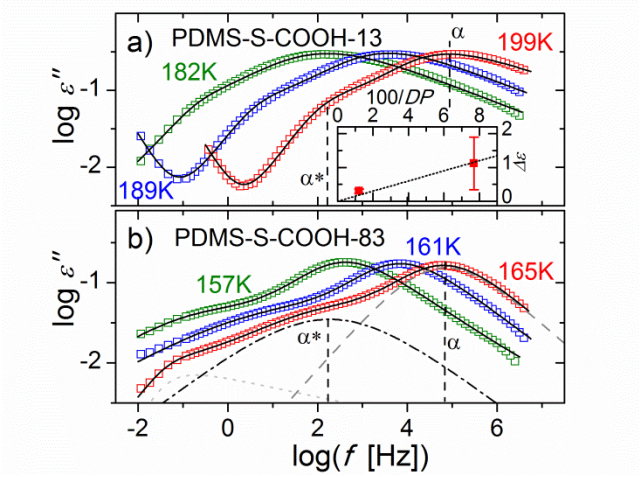

Figure 1: Dielectric loss spectra of (a) PDMS-COOH-13, and (b) PDMS-COOH-83 at different temperatures as indicated. At the higher temperatures the spectra of PDMS-S-COOH-13 exhibit a conductivity contribution at low frequencies while in PDMS-S-83 no such contribution was detected at the depicted frequencies. The solid lines are fits to the sum of two and three Havriliak-Negami functions, respectively; for PDMS-S-COOH-83, the three contributing functions are displayed separately as dashed, dash-dotted and dotted lines. The vertical dashed lines indicate the peak positions of the α- and α*-relaxation. The inset depicts the relaxation strength of the α*-relaxation averaged over several temperatures as function of the inverse *DP*; the dotted line indicates a 1/*DP* dependence and is a guide to the eye. The error bars reflect the variation of the extracted dielectric strength at different temperatures.

In the PDMS-S-COOH samples, a second relaxation process, separated by 2-3 orders in frequency from the segmental peak, exhibits a dielectric relaxation strength which decreases with increase in *DP* (compare the spectral shape in Fig. 1a and Fig. 1b). Its amplitude seems to scale linearly with inverse main chain length (Fig. 1, inset). This chain length dependence and its

general similarity to additional processes found in other associating polymers indicate its origin from the chain-ends, and we ascribe it to the chain end dissociation α*-relaxation, in agreement with previous studies[39,42]. The molecular assignment of the third relaxation process found at high temperatures in PDMS-S-COOH-83 is unclear and yet to be determined. However, this is out of the scope of this work and will not be discussed further.

In the case of PPG, the dipole moment is accumulated along the chain and chain modes appear in the dielectric spectra[42]. These dominate the dielectric spectra of PPG-NH_2 samples in the frequency range below the α-relaxation peak (Fig. 2). This obscures the α*-relaxation process since it is significantly weaker[42]. To sidestep this difficulty, the derivative of the permittivity spectra $\varepsilon'_{der}(\omega) = -\pi/2\ \partial\varepsilon'(\omega)/\partial\ \ln(\omega)$ can be used[45]. In this representation, the relaxation peaks are less broad, hence, it is generally easier to separate adjacent processes. Indeed, the ε'_{der} spectra of PPG-NH_2-6 and PPG-NH_2-67 exhibit the α*-relaxation as a shoulder of the α-relaxation and normal mode peak, respectively (Fig. 2). A sum of three Havriliak-Negami functions modified for the ε'_{der} spectra[45] was fit to these datasets in order to extract the characteristic relaxation times; a fit function composed of only two Havriliak-Negami peaks exhibits a systematic deviation from the spectra (Fig. S7). Additionally, this procedure enabled a fit of the α-relaxation peak of PPG-COOH-6, which in the loss spectra is obscured by the extremely strong α*-relaxation as described elsewhere[42]. However, in PPG-NH_2-33, the α*-relaxation could not be resolved since it is located probably extremely close to the normal mode peak. Consequently, the following analyses could not be done for this sample.

We would like to note that despite the association of several chains to longer super-chains the normal mode relaxation still indicates the chain dynamics of individual chains and not the super-chain. The reason is that for the normal mode to appear in dielectric spectra, each repeat unit must have a component of its dipole moment which is in parallel to the main chain, and additionally this component must be directed towards the same end of the chain in all repeat units. Only if the chemical structure of the polymer satisfies these conditions, the dipole moments can add up along the contour of the chain and give rise to an end-to-end dipole. In a super-chain, however, there is no mechanism which directs the end-to-end dipoles of the contributing chains towards the same end of the super-chain. Consequently, these end-to-end dipoles have random orientations towards both ends of the super-chain. Thus, on average the dipole moments along the super-chain cancel out.

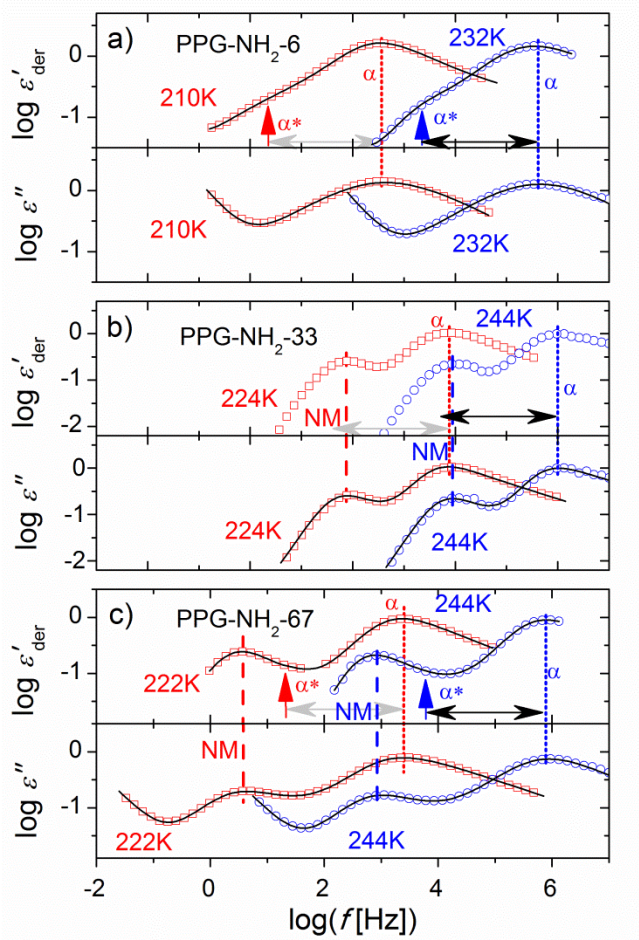

Figure 2: Dielectric permittivity derivative and loss spectra of (a) PPG-NH_2-6, (b) PPG-NH_2-33, and (c) PPG-NH_2-67 at different temperatures as indicated. The solid lines are fits to Havriliak-Negami functions; the dotted and dashed vertical lines indicate the position of the α-relaxation and normal mode (NM), respectively; the vertical arrows highlight the position of the α*-relaxation where it can be detected. The horizontal double-arrow approximates the separation between α- and α*-relaxation which indicates that in PPG-NH_2-33 the latter is at the same position as the normal mode, hence, it cannot be resolved.

Shear rheology

The shear modulus spectra were used to construct master curves by horizontally shifting the spectra by a shift factor $a(T)$ to match G' and G'' (Fig. 3). This, however, requires the assumption of time-temperature superposition (tTs) which is probably not entirely valid. Nevertheless, tTs was employed in past investigations of associating polymers[46-48] and has proven to be a useful tool to explore their dynamic processes. The first process occurs at high frequencies (corresponding to temperatures near T_g) and exhibits storage modulus values between 0.1 and 1 GPa; consequently, it is assigned to the segmental relaxation. The crossover of G' and G'' is used to determine the corresponding segmental relaxation time. In all investigated polymers a second process appears at lower frequencies, i.e. higher temperatures (Figs. 3, S5 & S6), although it is

demanding to separate it from the segmental relaxation in the samples with short chains. At even lower frequencies the distinctive slopes of 2 and 1 in G' and G'', respectively, are present in the double-logarithmic presentation (Fig. 3). These slopes are characteristic for the terminal relaxation, usually related to the motion of whole chains[41]. In these materials, however, the terminal relaxation occurs at times much longer than expected for their molecular weight, e.g. in PPG-NH_2-33 and PPG-COOH-33 the terminal relaxation is by about one and almost two decades, respectively, slower than in the methyl-terminated equivalent[42]. This observation indicates that the terminal relaxation reflects the mechanical enhancement due to the formation of a supramolecular network. To estimate the corresponding characteristic relaxation times we employed a simplified model function to fit the master curves[37]:

$$G'(\omega) = \frac{A}{(\omega\tau_1)^{b_1} + (\omega\tau_1)^{-b_2}} + G_e\frac{\omega^2\tau_2^2}{1+\omega^2\tau_2^2} \quad (7a)$$

$$G''(\omega) = \frac{A}{(\omega\tau_1)^{c_1} + (\omega\tau_1)^{-c_2}} + G_e\frac{\omega\tau_2}{1+\omega^2\tau_2^2} \quad (7b)$$

The first term phenomenologically describes the segmental relaxation with the constant A reflecting the level of G' (glassy modulus) and the area under G'', the characteristic relaxation time τ_1 which indicates the segmental relaxation time and the parameters b_1 and $-b_2$ as well as c_1 and $-c_2$ for the slopes of the high and low frequency wings of G' and G'', respectively. Even though, in general, this term does not fulfill the Kramers-Kronig relation, it provides a sufficiently accurate approximation to estimate the characteristic segmental relaxation time. The second term resembles a Maxwell model in order to describe the terminal relaxation where G_e and τ_2 are the corresponding plateau modulus and terminal relaxation time, respectively. For almost all samples, eq. (7a) and eq. (7b) were fit simultaneously to the G' and G'' data with shared parameters. However, in PPG-NH_2-6 this joint fit did not describe the data appropriately; in this case, only eq. (7b) was used to fit G'' to deduce the relaxation times (Fig. 3a).

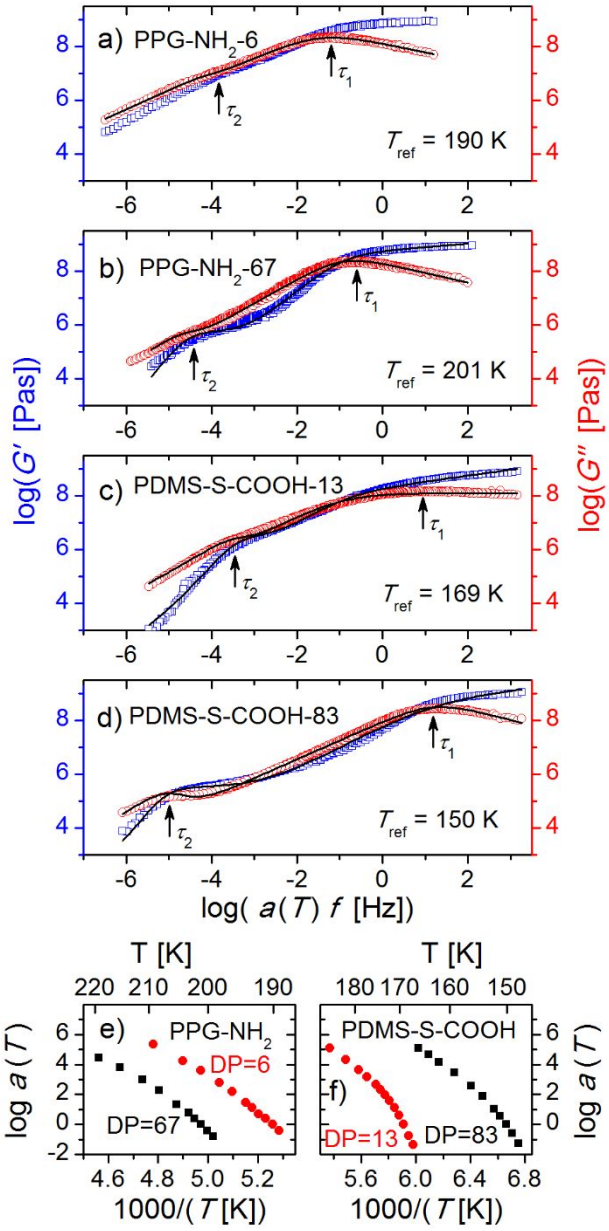

Figure 3: Examples of shear modulus master curves of (a) PPG-NH_2-6, (b) PPG-NH_2-67, (c) PDMS-S-COOH-13, (d) PDMS-S-COOH-83 as well as the respective shift factors $a(T)$ of (e) PPG-NH_2 and (f) PDMS-S-COOH used for the construction of the master curves as function of inverse temperature. The solid lines in panel (a) – (d) are fits to eq. (7) and the vertical arrows indicate the respective relaxation times τ_1 and τ_2.

With the shift factors $a(T)$ used to construct the master curves, the relaxation times $\tau(T_{ref})$ obtained from the fits of eq. (7), which refer to the reference temperature T_{ref}, can be converted into a set of relaxation times at different temperatures:

$$\tau(T) = \frac{\tau(T_{ref})}{a(T)} \tag{8}$$

We would like to point out that this procedure appears to provide relaxation time data in a range much larger than the dynamic range of the rheometer. However, since tTs cannot be considered valid in these materials, only the values of relaxation times which are within the rheometer's dynamic range at a given T are reliable, and only these values are used in our analysis. It is important to emphasize that the determination of $\tau(T_{ref})$ is based on the scaled angular frequency axis $a(T)\omega$. Consequently, the relaxation times deduced via eq. (8) are not affected by the choice of the shift factors as long as they are within the original dynamic range.

In most cases, the segmental relaxation times extracted from the shear modulus measurements are considerably smaller than the α-relaxation times obtained from the respective dielectric loss measurements (Fig. 4). Similar observations were reported in the literature[49-51] and were ascribed to the fact that shear modulus and dielectric loss are different types of physical quantities, i.e. modulus and compliance, respectively[37, 49]. This is also captured by the often-neglected fact that peaks in the former yield true relaxation times while the maxima in the latter should be considered retardation times. To prove that this difference is not an artifact from the different methods (e.g. altered sample preparation or treatment), for the examples of PPG-NH_2-67, PDMS-S-COOH-13 and PPG-COOH-67 we analyze also the imaginary part M'' of the complex dielectric modulus $M^* = M' + iM''$ which is related to the complex dielectric permittivity via the equation $M^* = 1/\varepsilon^*$. Comparing the relaxation times of the α-relaxation of both M'' and ε'' demonstrates (Fig. 4) that in the modulus spectra the peak appears at higher frequencies than in the corresponding permittivity loss spectra. This seems to be even more pronounced in very broad peaks[37].

The two fields, dielectric spectroscopy and rheology, have developed well established methods to analyze compliance and modulus data, respectively. Since these analysis methods are tailored to match the characteristic features of each of the two experimental techniques, we employ them in the conventional manner. This means that we analyze the (imaginary part of the) dielectric permittivity (a compliance) and the shear modulus to benefit from the well-founded approaches behind the respective analysis models. We would like to note that there are also practical issues suggesting this approach, namely the fact that α*-relaxation peak is less pronounced in the dielectric modulus spectra leading to less accurate data. In some samples it is even not resolvable – and equations to analyze the derivative spectra (like developed for the permittivity) have no analytical foundation). However, in order to compare the resulting relaxation times (since the term *relaxation time* is so established throughout the literature for what actually should be called retardation time, we will not distinguish between them in the following), we correct for the discrepancy by multiplying a correction factor C to the rheological relaxation times (Table 2). The factor C is chosen to match the rheological segmental relaxation times onto the dielectric α-relaxation times: $C\tau_1(T) = \tau_\alpha(T)$. In the following analyses, τ_c denotes the corrected terminal relaxation time $C\tau_2$. The correction factor C basically reflects the ratio of relaxation and retardation time which depends largely on the shape of the relaxation peak. Consequently, its

value is individual for each sample (Tab. 2). In almost all samples it is between half a decade to about one decade; only in PPG-NH_2-6 this range was exceeded with $C = 58$. This exceptionally high value is unlikely to be just the result of the difference between relaxation and retardation times; instead we presume that the rather broad shear modulus peak may inhibit an accurate determination of its characteristic time. Therefore, we exclude this sample from the following analyses.

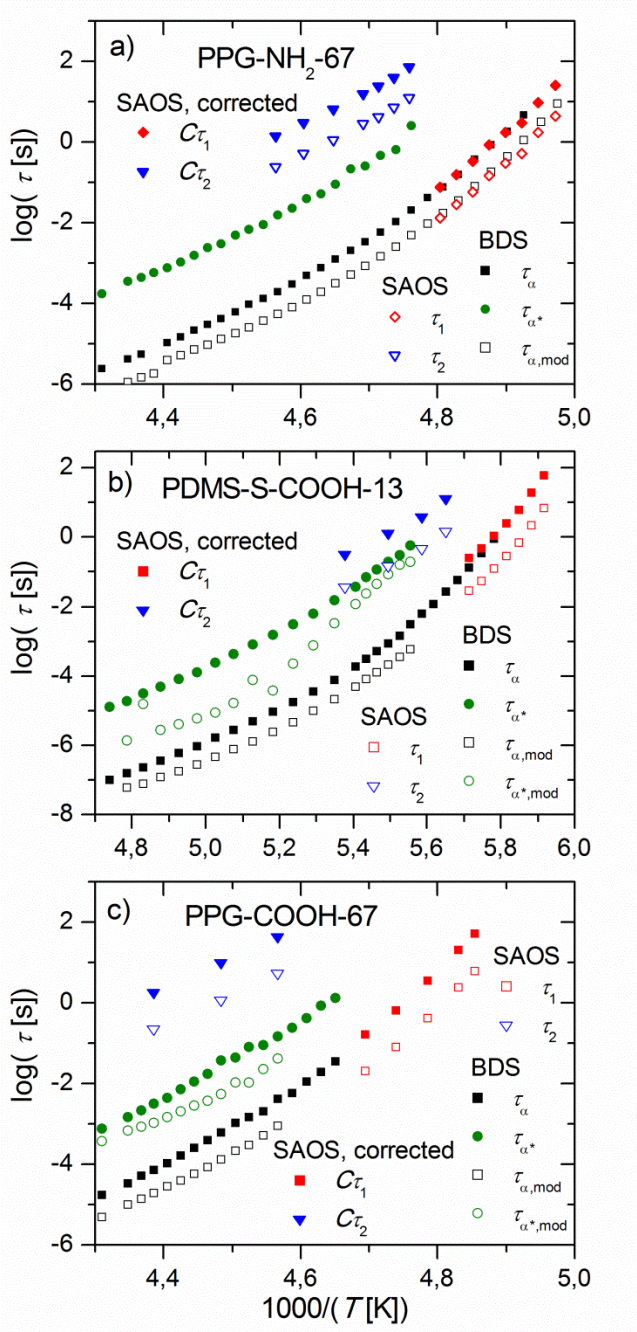

Figure 4: Activation plot of the relaxation times for (a) PPG-NH_2-67, (b) PDMS-S-COOH-13, and (c) PPG-COOH-67 extracted from dielectric loss (τ_α and $\tau_{\alpha*}$) and shear modulus measurements (segmental relaxation time τ_1 and terminal relaxation time τ_2) as well as the

dielectric modulus ($\tau_{\alpha,\mathrm{mod}}$ and $\tau_{\alpha^*,\mathrm{mod}}$). The corrected rheological relaxation times $C\tau_1$ and $C\tau_2$ were determined using the correction factor $C = \tau_\alpha/\tau_1$. The experimental uncertainty is smaller than the symbol size.

In all investigated polymers, the corrected rheological terminal relaxation time τ_c is larger than the dielectric α*-relaxation time τ_{α^*} (Figs. 4, 5), as is suggested by the model of bond lifetime renormalization[40]. Moreover, the separation increases with increasing MW for all examined main chain and end-group types; it is smaller than 1 decade for the shortest chains and ranges up to 4 decades in the longest ones. In contrast to the corrected rheological terminal relaxation times, the uncorrected ones τ_2 exhibit an implausible behavior ranging from faster than the dielectric α*-relaxation time τ_{α^*} to about equal and even much longer (Fig. 5).

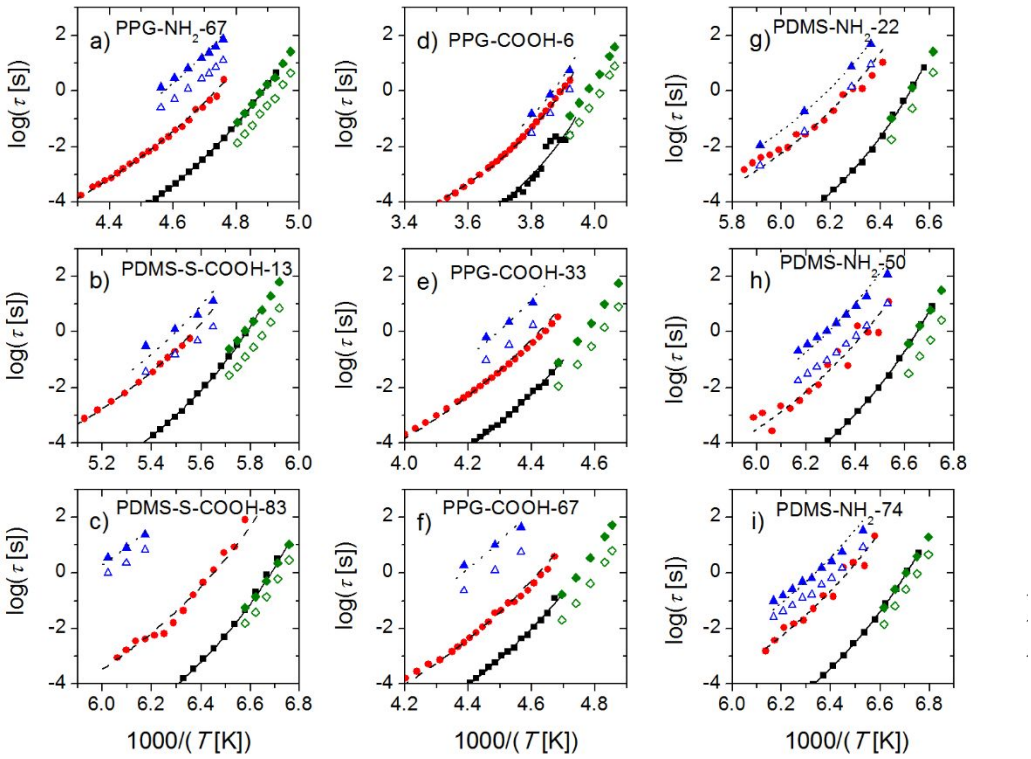

Figure 5: Activation plots of the mean relaxation time of the dielectric α- (black squares) and α*-relaxation (red circles) as well as the uncorrected (open blue triangles) and corrected rheological terminal relaxation (closed blue triangles) and the uncorrected (open green diamonds) and corrected rheological segmental relaxation (closed green diamonds) of (a) PPG-NH_2-67, (b) PDMS-S-COOH-13, (c) PDMS-S-COOH-83, (d) PPG-COOH-6, (e) PPG-COOH-33, (f) PPG-COOH-67, (g) PDMS-NH_2-22, (h) PDMS-NH_2-50, (i) PDMS-NH_2-74. The experimental uncertainty is smaller than the symbol size. Solid lines are fits of the dielectric segmental

relaxation to the VFT equation (eq. (6)); dashed lines are fits of the α*-relaxation time to eq. (1) using the VFT fit parameters of the respective α-relaxation and only E_a as a free fit parameter (Table 2); dotted lines are fits of the corrected terminal relaxation time to eq. (5) with fixed E_a and VFT parameters, and only the exponent x as a free fit parameter.

Since the terminal relaxation regime is strongly affected by the chain end association, we can expect strong changes also in the zero shear viscosity η_0. To compensate for the impact of different T_g the viscosities are evaluated as a function of inverse temperature scaled by the respective T_g (Fig. 6). In agreement with the previous results, all H-bonding samples exhibit a higher zero shear viscosity than their non-H-bonding counterparts. This also reflects the prolonged relaxation of mechanical stress due to the supramolecular network. Larger enhancements are found in the -COOH terminated chains for both PPG and PDMS as can be expected from the stronger H-bonding. Crystallization of PDMS prevents the viscosity measurements of many samples in the intermediate temperature range.

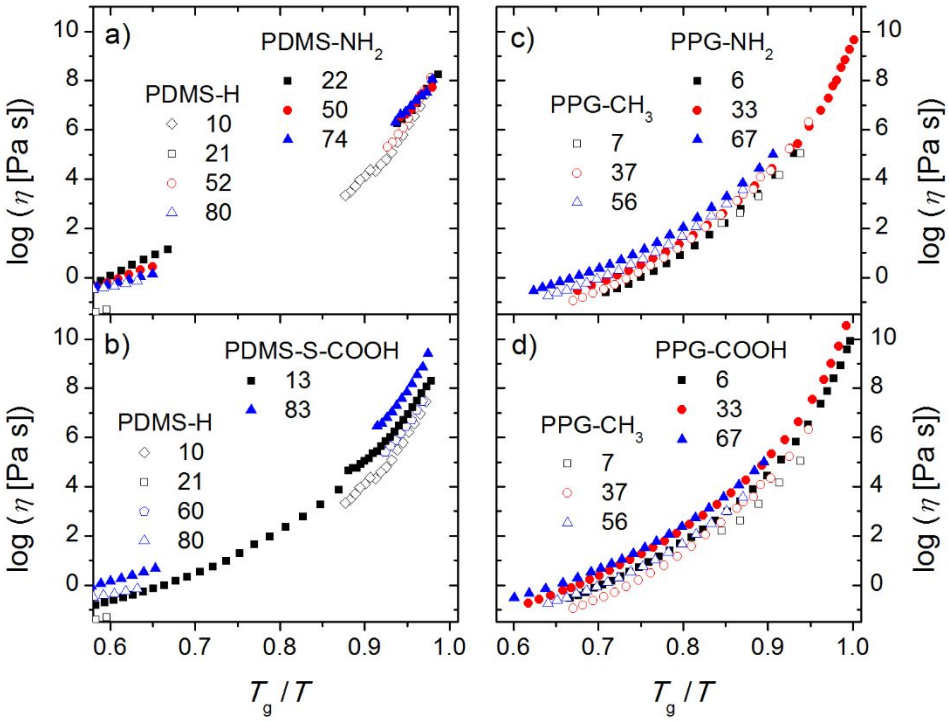

Figure 6: Zero shear viscosity *vs.* T_g-scaled inverse temperature of (a) PDMS-NH_2 and PDMS-H, (b) PDMS-S-COOH and PDMS-H, (c) PG-NH_2 and PPG-CH_3, and (d) PPG-COOH and PPG-CH_3 of different *DP* as indicated by numbers.

Discussion

Following the assignment that the α*-relaxation reflects single dissociation events of end-groups[38], we can use the VFT parameters obtained from the α-relaxation via eq. (6) to set $\tau_\alpha(T)$

and fit eq. (1) to the $\tau_{\alpha*}(T)$ data with E_a as the only free parameter (Fig. 5). The resulting activation energies of the dissociation process are about 6 kJ/mol for PPG-NH_2-6, 7-9 kJ/mol for PPG-NH_2-67, PPG-COOH, PDMS-NH_2 and PDMS-S-COOH (Table 2).

Table 2: VFT fit parameters of the α-relaxation, activation energies of the α*-relaxation according to eq. (1) when the latter was detectable, the correction factor C of the rheological relaxation times and the diffusion exponent x. The energy $2\,k_BT\ln N$ indicates the threshold between the intermediate and strong interaction regime (see text).

Sample	$\log(\tau_0$ [s])	B [K]	T_0 [K]	E_a [kJ/mol]	$2\,k_BT\ln N$ [kJ/mol]	C	x
PPG-NH_2-6	-13.2	1128	160	5.8±0.1	3.9	58	-
PPG-NH_2-67	-12.8	1022	170	8.1±0.1	12.9	5.7	0.36±0.006
PPG-COOH-6	-9.9	633	223	8.4±0.2	4.8	4.9	0.49±0.03
PPG-COOH-33	-12.6	1129	180	8.5±0.1	11.2	6.9	0.37±0.01
PPG-COOH-67	-13.9	1302	169	7.3±0.1	13.4	8.3	0.28±0.01
PDMS-NH_2-22	-12.1	516	135	9.1±0.2	5.6	5.7	0.47±0.005
PDMS-NH_2-50	-13.5	657	129	7.6±0.3	7.8	12	0.39±0.01
PDMS-NH_2-74	-13.8	688	127	8.3±0.2	8.8	4.1	0.43±0.01
PDMS-S-COOH-13	-11.5	700	147	8.2±0.4	4.3	8.7	0.48±0.04
PDMS-S-COOH-83	-13.6	679	128	8.1±0.2	9.2	3.7	0.23±0.002

A close inspection of the $\tau_{\alpha*}(T)$ data and the respective fits to eq. (1) reveals a slight but systematic deviation (Fig. 5), with the temperature dependence of the experimental $\tau_{\alpha*}(T)$ in several samples being slightly weaker than expected. This suggests that the chosen description is missing a contribution. Introducing a temperature dependent activation energy of the dissociation process could resolve this issue; however, this is rather unlikely since E_a can be considered, in first approximation, temperature independent. In contrast, assuming $\tau_\alpha(T)$ as pre-factor in eq. (1) is a quite coarse approximation since it reflects the average segmental relaxation time dominated by the segments which are not located at the ends of the chain. However, the relevant timescale for the dissociation event is the segmental relaxation time of the end group, which can differ significantly from the average segmental relaxation time due to chemically different linker groups, or simply due to the usually enhanced mobility of chain ends. Nevertheless, for the following analyses we assume that $\tau_\alpha(T)$ represents a sufficiently accurate approximation to determine reasonable values of E_a.

With the obtained values of E_a (Table 2) we can relate a bond strength regime to each sample considering the criterion for intermediate bond strength, $k_BT\ln N < E_a < 2\,k_BT\ln N$. For that, the number of segments in the chain N (Table 1) is obtained from the DP and the characteristic ratio

C_∞ (6.3 for PDMS[52] and 5.76 for PPG[53]) according to $N = n/C_\infty$ where n denotes the number of atomic bonds in the main chain[54] (n equals to $2\times DP$ in PDMS and $3\times DP$ in PPG). For this estimates the temperature is taken to be $T_g + 20$ K. According to this criterion, the samples PPG-COOH-6, PDMS-NH_2-22, PDMS-S-COOH-13, are all forming strong bonds ($E_a > 2\, k_B T \ln N$) with the prediction $\tau_c \approx \tau_{\alpha^*}$. The experimental data indeed reveal a near-match of τ_c and τ_{α^*} for these materials (Figs. 5 a, c & i) in good agreement with the model prediction.[40]

However, most of the samples studied here are indeed in this intermediate regime (PPG-NH_2-67, PPG-COOH-33, PPG-COOH-67, PDMS-NH_2-50, PDMS-NH_2-74, PDMS-S-COOH-83). In that case the terminal relaxation time τ_c and the α*-relaxation time τ_{α^*} should differ (eq. 5), and their ratio τ_c/τ_{α^*} should depend only on chain length N, activation energy E_a and temperature T. For most of the samples, the measured data sets of τ_c and τ_{α^*} overlap only in a narrow temperature range. Hence, we neglect the impact of temperature and average over the available range to reduce the experimental uncertainty. The data show a clear trend of an increasing ratio τ_c/τ_{α^*} with increase of molecular weight from less than a half decade to about 4 decades (Fig. 7a), in a qualitative agreement with the model predictions (eq. 5). To provide a more quantitative comparison, we chose the Rouse regime ($x = 0.5$) and assume the activation energy $E_a = 8$ kJ/mol, the value close to the estimated E_a in most of the studied samples (Table 2). The behavior predicted by the model (eq. 5) indeed gives a reasonable quantitative description but only for short chains. As MW increases the data clearly deviate from this prediction (Fig. 7a). However, if we assume the reptation regime ($x = 0.25$) for the chain end diffusion, eq. (5) predicts a significantly larger τ_c/τ_{α^*} ratio (Fig. 7a). We want to emphasize that the prediction for reptation dynamics is estimated assuming T=200K, and it increases slightly upon cooling. The experimental data points are between these two predictions and approach the reptation regime at higher MW. Apparently, this suggests a transition from the prediction for Rouse dynamics to that for reptation dynamics with increase in MW. However, this transition appears at very short MW ~ 4 kg/mol (~30-40 Kuhn segments) in the case of PPG and ~6 kg/mol (~20-30 Kuhn segments) in PDMS. This is significantly below the critical MW M_c of PPG ($M_c = 7.7$ kg/mol[55]) and PDMS ($M_c = 24.5$ kg/mol[55]). These results indicate that the mechanical stress release might involve the relaxation of supramolecular chains with an effective MW larger than M_c even though the individual main chains are shorter[56].

For the sake of completeness, we did the same analysis also with the uncorrected rheological terminal relaxation times (i.e. τ_2 instead of τ_c). As mentioned before, in extremely short chains, these relaxation times are even faster than the α*-relaxation time. Although the chain length dependence of the ratio τ_2/τ_{α^*} is qualitatively similar ratio τ_c/τ_{α^*} (i.e. using the corrected data), for many samples the value of τ_2/τ_{α^*} is below the model prediction using Rouse dynamics (Fig. 7b). While earlier we pointed out the fundamental discrepancy which motivated the correction (Fig. 4), these results demonstrate that it cannot be neglected, instead it is necessary to obtain reasonable results.

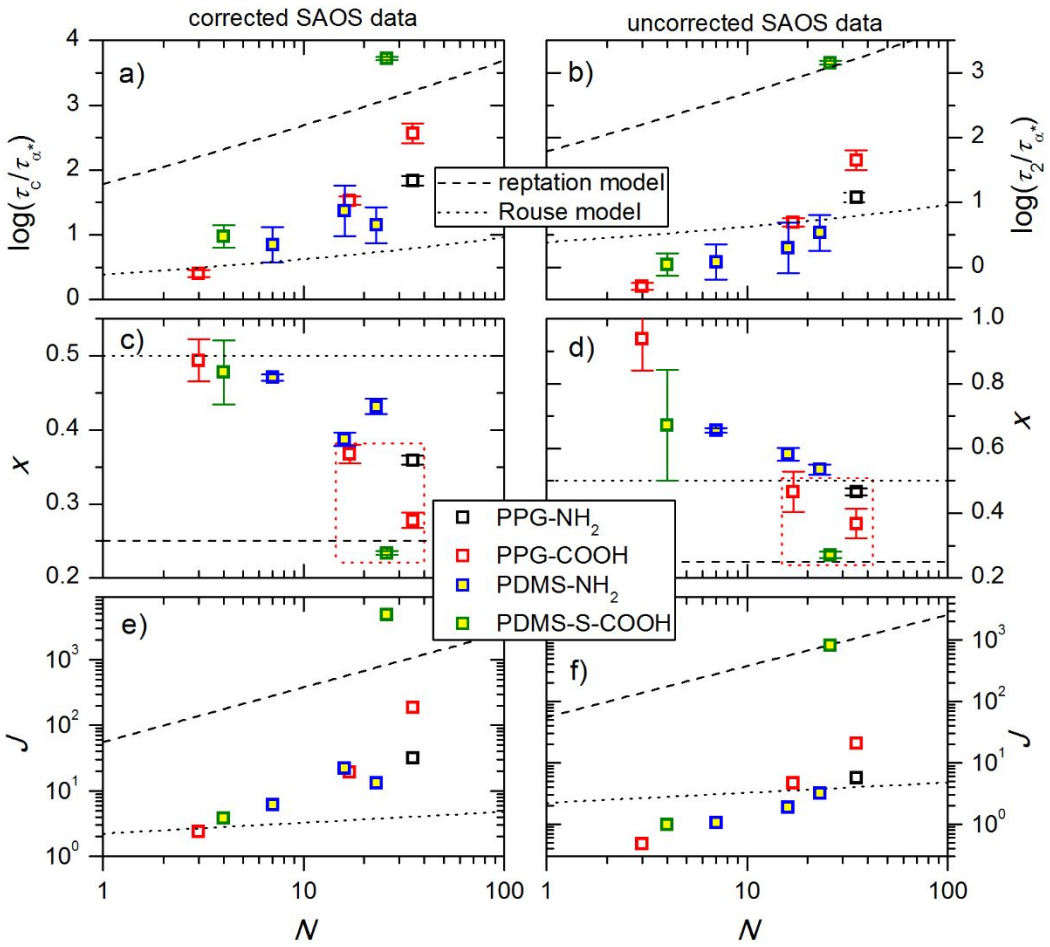

Figure 7: a) Ratio $\tau_c/\tau_{\alpha*}$ as function of the number of segments N of the main chain (based on the corrected SAOS data) and b) corresponding plot for the ratio $\tau_2/\tau_{\alpha*}$ (based on the uncorrected SAOS data). Random walk exponent x as a function of N based on c) the corrected and d) the uncorrected SAOS data. Number of returns J as a function of N based on e) the corrected and f) the uncorrected SAOS data. If not indicated, the experimental uncertainty is smaller than the symbol size. The dashed and dotted lines are the predictions of the lifetime renormalization model according to eq. (5) for reptation ($x = 0.25$) and Rouse ($x = 0.5$) dynamics, respectively, using an activation energy of E_a = 8 kJ/mol and a temperature of $T = 200$ K. The red boxes in panels c) and d) highlight the samples for which the effective MW of the super-chains deduced from viscosity is larger than M_c (see text for details).

Since we assign the rheological terminal relaxation to the stress relaxation from the supramolecular network, $\tau_c = \tau_b^{renm}$, we can use the model description of the normalized bond lifetime, i.e. eq. (5) to fit its temperature dependence (Fig. 5). To do that, we use the results of $\tau_\alpha(T)$ and E_a from the fits to the corresponding dielectric data sets as fixed values; the only free fit parameter in this procedure is the diffusion exponent x. The thus obtained x values exhibit a pronounced dependence on the chain length (Fig. 7c): in PPG-COOH-6, one of the shortest investigated chains, it has a value of 0.49 which indicates Rouse dynamics. It decreases with increasing number of segments until it reaches 0.23 in PDMS-S-COOH-83, the longest

investigated polymer. The latter value is close to 0.25, characteristic for reptation dynamics, which is expected to occur not until the critical MW M_c is exceeded. A similar observation has been reported for randomly functionalized polymers where x was found to be ~0.35 although the average separation along the backbone between adjacent associating functionalities was shorter than M_c[35, 36].

With the values of E_a and x obtained from the fitting of the dielectric and rheological data, respectively, the number of returns J can be calculated using eq. (4). As MW of the chain increases from 400 to 6000 (i.e. by about 1 decade), J increases from ~3 to more than 10^4 (Fig. 7e). This tremendous increase exceeds by far the scaling one may deduce from eq. (4) for either one of the two regimes, i.e. $J \sim N^{1/6}$ for Rouse dynamics and $J \sim N^{5/6}$ in the reptation regime. However, it can be explained by a transition between the two regimes since in that case the pre-factor increases from $\exp[E_a/(6RT)]$ to $\exp[5E_a/(6RT)]$.

Using the uncorrected rheological terminal relaxation times to determine x and J yields qualitatively similar trends as using τ_c. However, the absolute values for x are unphysically large (Fig. 7d) which would mean a chain end diffusion that exceeded Rouse dynamics by far. In contrast, the thus obtained values for J are much smaller while they still suggest a transition from Rouse to reptation dynamics.

Although we have no means to verify the values of x and J in order to check whether the bond lifetime renormalization model describes the molecular mechanisms in the investigated associating polymers, we can use their trend to perform an evaluation. In particular, the transition from Rouse to reptation like exponents x at chain length well below the entanglement length can only be explained by the formation of super-chains of a certain length. To evaluate whether this is the case, we make use of the fact that the zero shear viscosity can be linked to the chain length[57]. In the Rouse regime, the zero-shear viscosity is considered proportional to chain length. Hence, the viscosity of a super-chain comprised of n chains based on the viscosity η_1 of the non-associating chains is $n\eta_1$. Then, we can estimate how many chains are on average effectively joint in a super-chain, i.e. the association number, by dividing the T_g-scaled zero shear viscosity of each associating species by that one of their non-associating counterpart of similar MW. Using the obtained association numbers one can calculate the effective MW of the super-chains (Table 3). It turns out that for most of the materials, the effective MW of the super-chain is still below M_c; only for PPG-NH_2-67, PPG-COOH-33, PPG-COOH-67 and PDMS-S-COOH-83 it is larger. These samples also exhibit the smallest values of x (Fig. 7b) indicating reptation-like (entangled) dynamics. Thus, the transition from Rouse-like dynamics to reptation-like dynamics observed from the fit of experimental data to the bond lifetime renormalization model seems to be justified by the formation of supramolecular structures.

Table 3: Association number $N(\eta)$ and effective super-chain MW $M_w^{sc}(\eta)$ obtained from viscosity.

Polymer	$N(\eta)$	$M_w^{sc}(\eta)$ [kg/mol]
PPG-NH_2-67	4.8	19.4
PPG-COOH-6	6.5	4.4
PPG-COOH-33	8.3	18.7
PPG-COOH-67	2.1	8.8
PDMS-NH_2-22	4.7	8.2
PDMS-NH_2-50	2.0	7.8
PDMS-NH_2-74	1.8	9.5
PDMS-S-COOH-13	2.9	3.6
PDMS-S-COOH-83	3.3	21.4

Conclusion

Telechelic PDMS and PPG of different molecular weight (all below the entanglement molecular weight) with two types of dimer-forming H-bonding end groups (amide and carboxylic acid) were investigated by dielectric spectroscopy and linear shear rheology. The former method reveals the segmental motion (α-relaxation) as well as the dissociation process of the H-bonds at the end groups, i.e. the α*-relaxation which is several orders of magnitude slower. Following past publications, this separation reflects the H-bond dissociation energy[28]. In the shear modulus spectra, we find a terminal relaxation which indicates macroscopic stress relaxation in the system. However, its characteristic time τ_c is much longer than both the terminal relaxation expected for chains of that length as well as the bond dissociation time τ_{α^*} deduced from the dielectric spectroscopy. Such a divergence of bond dissociation time and stress relaxation has been reported in previous investigations of entangled, randomly functionalized polymers[35, 36], and is predicted by the bond lifetime renormalization model[40]. This model differentiates the bond dissociation process and the mechanical stress relaxation process that requires an exchange of sticker partners. The latter involves multiple dissociations and returns of the sticker to the initial bond partner including re-bonding events (which do not release mechanical stress) before it finds another sticker via a random walk, and in this way relaxes the mechanical stress. The model can be expanded by a random walk exponent x which takes into account the transition from Rouse to reptation dynamics.

Our detailed analysis demonstrated good agreement of the experimental data with the predictions of the bond lifetime renormalization model. The terminal relaxation time appears to be close to the dissociation time in case of strong interactions (short chains), and the difference of these two times increases strongly with MW. These results agree well with the model predictions assuming a transition to reptation-like dynamics even for chains that are much shorter than the critical MW. This indicates the formation of super-chains. An analysis of the viscosities indeed suggests the formation of such super-chains for the samples where the random walk exponent $x \sim 0.25$ (indicative for reptation dynamics) was found. We would like to stress that a more thorough

quantitative test of the bond lifetime renormalization model requires independent measurements of the exponent x and the number of returns J.

Acknowledgement

This work was supported by the NSF Polymer program under grant DMR-1408811. MT is grateful to the Alexander von Humboldt Foundation for granting him a Feodor-Lynen fellowship. PC and TS acknowledge partial financial support for polymer synthesis by the U.S. Department of Energy, Office of Science, Basic Energy Sciences, Materials Science & Engineering Division.

References

1. Brunsveld, L.; Folmer, B.; Meijer, E. W.; Sijbesma, R. Supramolecular polymers. *Chemical Reviews* **2001,** 101 (12), 4071-4098.
2. Monkenbusch, M.; Krutyeva, M.; Pyckhout-Hintzen, W.; Antonius, W.; Hovelmann, C. H.; Allgaier, J.; Bras, A.; Farago, B.; Wischnewski, A.; Richter, D. Molecular View on Supramolecular Chain and Association Dynamics. *Phys Rev Lett* **2016,** 117 (14), 147802.
3. Bauer, S.; Stern, J.; Böhm, F.; Gainaru, C.; Havenith, M.; Loerting, T.; Böhmer, R. Vibrational study of anharmonicity, supramolecular structure, and hydrogen bonding in two octanol isomers. *Vibrational Spectroscopy* **2015,** 79, 59-66.
4. Feldman, K. E.; Kade, M. J.; Meijer, E. W.; Hawker, C. J.; Kramer, E. J. Model Transient Networks from Strongly Hydrogen-Bonded Polymers. *Macromolecules* **2009,** 42 (22), 9072-9081.
5. Kulkarni, A.; Lele, A.; Sivaram, S.; Rajamohanan, P. R.; Velankar, S.; Chatterji, A. Star Telechelic Poly(l-lactide) Ionomers. *Macromolecules* **2015,** 48 (18), 6580-6588.
6. Lundberg, R. D.; Makowski, H. S.; Westerman, L., The Dual Plasticization of Sulfonated Polystyrene Ionomer. In *Ions in Polymers*, 1980; pp 67-76.
7. Tang, S.; Olsen, B. D. Relaxation Processes in Supramolecular Metallogels Based on Histidine–Nickel Coordination Bonds. *Macromolecules* **2016,** 49 (23), 9163-9175.
8. Li, S.-L.; Xiao, T.; Lin, C.; Wang, L. Advanced supramolecular polymers constructed by orthogonal self-assembly. *Chemical Society Reviews* **2012,** 41 (18), 5950-5968.
9. Xing, K.; Chatterjee, S.; Saito, T.; Gainaru, C.; Sokolov, A. P. Impact of hydrogen bonding on dynamics of hydroxyl-terminated Polydimethylsiloxane. *Macromolecules* **2016,** 49 (8), 3138-3147.
10. Cao, P. F.; Li, B.; Hong, T.; Townsend, J.; Qiang, Z.; Xing, K.; Vogiatzis, K. D.; Wang, Y.; Mays, J. W.; Sokolov, A. P. Superstretchable, Self - Healing Polymeric Elastomers with Tunable Properties. *Advanced Functional Materials* **2018,** 28 (22), 1800741.
11. Schubert, C.; Dreier, P.; Nguyen, T.; Maciol, K.; Blankenburg, J.; Friedrich, C.; Frey, H. Synthesis of linear polyglycerols with tailored degree of methylation by copolymerization and the effect on thermorheological behavior. *Polymer* **2017,** 121, 328-339.
12. Cordier, P.; Tournilhac, F.; Soulie-Ziakovic, C.; Leibler, L. Self-healing and thermoreversible rubber from supramolecular assembly. *Nature* **2008,** 451 (7181), 977-980.
13. Campanella, A.; Döhler, D.; Binder, W. H. Self-Healing in Supramolecular Polymers. *Macromolecular Rapid Communications* **2018**, 39, 1700739.
14. Huang, Y.-F.; Xu, J.-Z.; Xu, J.-Y.; Zhang, Z.-C.; Hsiao, B. S.; Xu, L.; Li, Z.-M. Self-reinforced polyethylene blend for artificial joint application. *Journal of Materials Chemistry B* **2014,** 2 (8), 971-980.
15. Li, J.; Viveros, J. A.; Wrue, M. H.; Anthamatten, M. Shape-Memory Effects in Polymer Networks Containing Reversibly Associating Side-Groups. *Advanced Materials* **2007,** 19 (19), 2851-2855.
16. Noro, A.; Hayashi, M.; Matsushita, Y. Design and properties of supramolecular polymer gels. *Soft Matter* **2012,** 8 (24), 6416-6429.

17. Goldansaz, H.; Fustin, C.-A.; Wübbenhorst, M.; van Ruymbeke, E. How Supramolecular Assemblies Control Dynamics of Associative Polymers: Toward a General Picture. *Macromolecules* **2016,** 49 (5), 1890-1902.
18. Chen, Q.; Zhang, Z.; Colby, R. H. Viscoelasticity of entangled random polystyrene ionomers. *Journal of Rheology* **2016,** 60 (6), 1031-1040.
19. Ng, W. K.; Tam, K. C.; Jenkins, R. D. Lifetime and network relaxation time of a HEUR-C20 associative polymer system. *Journal of Rheology* **2000,** 44 (1), 137-147.
20. Knaebel, A.; Skouri, R.; Munch, J. P.; Candau, S. J. Structural and rheological properties of hydrophobically modified alkali-soluble emulsion solutions. *Journal of Polymer Science Part B: Polymer Physics* **2002,** 40 (18), 1985-1994.
21. Liao, D.; Dai, S.; Tam, K. C. Rheological properties of hydrophobic ethoxylated urethane (HEUR) in the presence of methylated β-cyclodextrin. *Polymer* **2004,** 45 (25), 8339-8348.
22. Manassero, C.; Raos, G.; Allegra, G. Structure of Model Telechelic Polymer Melts by Computer Simulation. *Journal of Macromolecular Science, Part B* **2007,** 44 (6), 855-871.
23. Manassero, C.; Castellano, C. Telechelic Melt Polymer's Structure Variation Depending on Shear Deformation. *Journal of Macromolecular Science, Part B* **2013,** 52 (10), 1465-1477.
24. Zhuge, F.; Hawke, L. G. D.; Fustin, C.-A.; Gohy, J.-F.; van Ruymbeke, E. Decoding the linear viscoelastic properties of model telechelic metallo-supramolecular polymers. *Journal of Rheology* **2017,** 61 (6), 1245-1262.
25. Park, G. W.; Ianniruberto, G. A new stochastic simulation for the rheology of telechelic associating polymers. *Journal of Rheology* **2017,** 61 (6), 1293-1305.
26. Meng, X.-X.; Russel, W. B. Rheology of telechelic associative polymers in aqueous solutions. *Journal of Rheology* **2006,** 50 (2), 189-205.
27. Ozaki, H.; Koga, T. Network Formation and Mechanical Properties of Telechelic Associating Polymers with Fixed Junction Multiplicity. *Macromolecular Theory and Simulations* **2017,** 26 (2), 1600076.
28. Chen, Q.; Tudryn, G. J.; Colby, R. H. Ionomer dynamics and the sticky Rouse model. *Journal of Rheology* **2013,** 57 (5), 1441-1462.
29. Chen, Q.; Huang, C.; Weiss, R. A.; Colby, R. H. Viscoelasticity of Reversible Gelation for Ionomers. *Macromolecules* **2015,** 48 (4), 1221-1230.
30. Zhang, Z.; Huang, C.; Weiss, R. A.; Chen, Q. Association energy in strongly associative polymers. *Journal of Rheology* **2017,** 61 (6), 1199-1207.
31. Tanaka, F.; Edwards, S. Viscoelastic properties of physically crosslinked networks. 1. Transient network theory. *Macromolecules* **1992,** 25 (5), 1516-1523.
32. Tanaka, F.; Edwards, S. Viscoelastic properties of physically crosslinked networks: Part 1. Non-linear stationary viscoelasticity. *Journal of Non-Newtonian Fluid Mechanics* **1992,** 43 (2-3), 247-271.
33. Indei, T. Rheological study of transient networks with junctions of limited multiplicity. *J Chem Phys* **2007,** 127 (14), 144904.
34. Indei, T. Rheological study of transient networks with junctions of limited multiplicity. II. Sol/gel transition and rheology. *J Chem Phys* **2007,** 127 (14), 144905.
35. Gold, B. J.; Hövelmann, C. H.; Lühmann, N.; Székely, N. K.; Pyckhout-Hintzen, W.; Wischnewski, A.; Richter, D. Importance of Compact Random Walks for the Rheology of Transient Networks. *ACS Macro Letters* **2017,** 6 (2), 73-77.
36. Gold, B. J.; Hövelmann, C. H.; Lühmann, N.; Pyckhout-Hintzen, W.; Wischnewski, A.; Richter, D. The microscopic origin of the rheology in supramolecular entangled polymer networks. *Journal of Rheology* **2017,** 61 (6), 1211-1226.
37. Kremer, F.; Schönhals, A., *Broadband Dielectric Spectroscopy*. Springer Science & Business Media: 2012.

38. Müller, M.; Fischer, E.; Kremer, F.; Seidel, U.; Stadler, R. The molecular dynamics of thermoreversible networks as studied by broadband dielectric spectroscopy. *Colloid and Polymer Science* **1995,** 273 (1), 38-46.
39. Xing, K.; Tress, M.; Cao, P.; Cheng, S.; Saito, T.; Novikov, V. N.; Sokolov, A. P. Hydrogen-bond strength changes network dynamics in associating telechelic PDMS. *Soft Matter* **2018,** 14, 1235-1246.
40. Stukalin, E. B.; Cai, L. H.; Kumar, N. A.; Leibler, L.; Rubinstein, M. Self-Healing of Unentangled Polymer Networks with Reversible Bonds. *Macromolecules* **2013,** 46 (18), 7525-7541.
41. Wang, S.-Q., *Nonlinear Polymer Rheology: Macroscopic Phenomenology and Molecular Foundation*. John Wiley & Sons: 2018.
42. Xing, K.; Tress, M.; Cao, P.-F.; Fan, F.; Cheng, S.; Saito, T.; Sokolov, A. P. The Role of Chain-End Association Lifetime in Segmental and Chain Dynamics of Telechelic Polymers. *Macromolecules* **2018,** 51 (21), 8561-8573.
43. Wagner, H.; Richert, R. Equilibrium and non-equilibrium type β-relaxations: d-sorbitol versus o-terphenyl. *The Journal of Physical Chemistry B* **1999,** 103 (20), 4071-4077.
44. Havriliak, S.; Negami, S. A complex plane representation of dielectric and mechanical relaxation processes in some polymers. *Polymer* **1967,** 8, 161-210.
45. Wübbenhorst, M.; Van Turnhout, J. Analysis of complex dielectric spectra. I. One-dimensional derivative techniques and three-dimensional modelling. *Journal of Non-Crystalline Solids* **2002,** 305 (1-3), 40-49.
46. Shabbir, A.; Javakhishvili, I.; Cerveny, S.; Hvilsted, S.; Skov, A. L.; Hassager, O.; Alvarez, N. J. Linear viscoelastic and dielectric relaxation response of unentangled UPy-based supramolecular networks. *Macromolecules* **2016,** 49 (10), 3899-3910.
47. Yanagisawa, Y.; Nan, Y.; Okuro, K.; Aida, T. Mechanically robust, readily repairable polymers via tailored noncovalent cross-linking. *Science* **2018,** 359 (6371), 72-76.
48. Herbst, F.; Schröter, K.; Gunkel, I.; Gröger, S.; Thurn-Albrecht, T.; Balbach, J.; Binder, W. H. Aggregation and chain dynamics in supramolecular polymers by dynamic rheology: cluster formation and self-aggregation. *Macromolecules* **2010,** 43 (23), 10006-10016.
49. Nicolai, T.; Floudas, G. Dynamics of linear and star poly (oxypropylene) studied by dielectric spectroscopy and rheology. *Macromolecules* **1998,** 31 (8), 2578-2585.
50. Nicol, E.; Nicolai, T.; Durand, D. Dynamics of poly (propylene sulfide) studied by dynamic mechanical measurements and dielectric spectroscopy. *Macromolecules* **1999,** 32 (22), 7530-7536.
51. Hofmann, M.; Gainaru, C.; Cetinkaya, B.; Valiullin, R.; Fatkullin, N.; Rössler, E. Field-cycling relaxometry as a molecular rheology technique: common analysis of NMR, shear modulus and dielectric loss data of polymers vs dendrimers. *Macromolecules* **2015,** 48 (20), 7521-7534.
52. Ding, Y.; Sokolov, A. P. Comment on the dynamic bead size and Kuhn segment length in polymers: Example of polystyrene. *Journal of Polymer Science Part B: Polymer Physics* **2004,** 42 (18), 3505-3511.
53. Kokubo, S.; Vana, P. Easy Access to the Characteristic Ratio of Polymers Using Ion-Mobility Mass Spectrometry. *Macromolecular Chemistry and Physics* **2017,** 218 (1), 1600373.
54. Rubinstein, M.; Colby, R. H., *Polymer physics*. Oxford university press New York: 2003; Vol. 23.
55. Zang, Y. H.; Carreau, P. J. A correlation between critical end - to - end distance for entanglements and molecular chain diameter of polymers. *Journal of applied polymer science* **1991,** 42 (7), 1965-1968.
56. Leibler, L.; Rubinstein, M.; Colby, R. Dynamics of telechelic ionomers. Can polymers diffuse large distances without relaxing stress? *Journal de Physique II* **1993,** 3 (10), 1581-1590.
57. Krutyeva, M.; Brás, A.; Antonius, W.; Hövelmann, C.; Poulos, A.; Allgaier, J.; Radulescu, A.; Lindner, P.; Pyckhout-Hintzen, W.; Wischnewski, A.; Richter, D. Association Behavior, Diffusion, and

Viscosity of End-Functionalized Supramolecular Poly (ethylene glycol) in the Melt State. *Macromolecules* **2015,** 48 (24), 8933-8946.

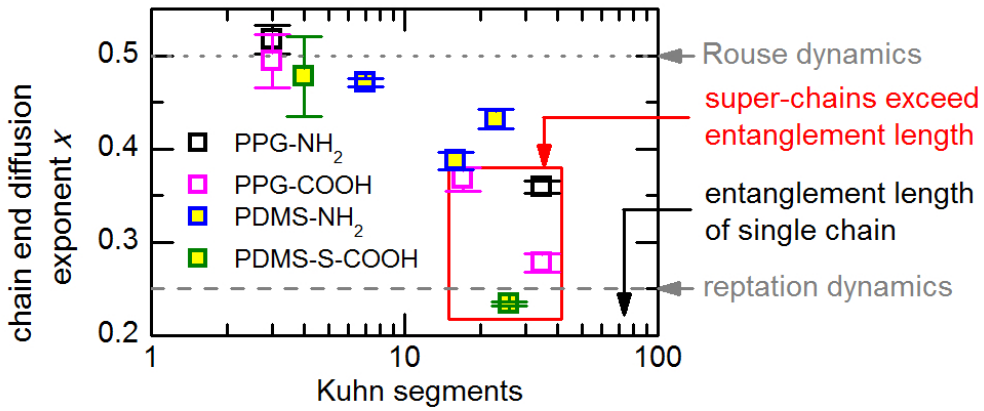

82x34mm (300 x 300 DPI)